




Muhittin Turan 

Bending analysis of two-directional functionally graded beams using trigonometric series functions

Received: 23 November 2021 / Accepted: 24 March 2022 / Published online: 21 April 2022
© The Author(s), under exclusive licence to Springer-Verlag GmbH Germany, part of Springer Nature 2022

Abstract In the present paper, Navier’s method based on the first-order shear deformation theory for bending analysis of two-directional functionally graded beams subjected to various sets of boundary conditions is presented. In Navier’s method, different trigonometric series functions are proposed for each boundary condition. The accuracy of these proposed functions was investigated and compared with the literature. It is also presented in a parametric study. The governing equations are derived according to Lagrange’s principle. The variation of the components of the beam material in the volume is defined by a power-law rule. The normalized maximum transverse deflections, the normalized axial and transverse shear stresses are obtained for various boundary conditions, gradation exponents (p_x, p_z) in the x - and z -directions, and the slenderness (L/h). The trigonometric series functions used in this study give results that are quite compatible with the literature. In addition, the parametric study contributes to the literature.

Keywords Two-directional functionally graded materials · Navier’s method · Bending analysis · First-order shear deformation theory · Trigonometric series functions

1 Introduction

Functionally graded materials (FGMs), which have wide usage areas such as aviation, aircraft and space industry, mechanical, construction, and electrical circuit industry, are preferred because they are highly resistant to thermal changes. Its mechanical properties change smoothly and continuously from one side to the other. It is formed of ceramic and metal phases to reduce thermal stresses due to temperature changes. Due to the constant change in the composition of the component materials, FGMs have many advantages over composites. Therefore, many researchers have studied the mechanical behavior of FGMs.

According to the literature, researchers have conducted a significant number of studies over the past two decades to predict and understand the bending, buckling, and vibration behavior of conventional (one-directional) functionally graded beams (or 1D-FGBs) and plates based on different theories [1–18].

1D-FGMs are unsuitable for meeting technical requirements such as temperature and stress distributions in two or three directions for spacecraft and shuttles. To eliminate the mentioned disadvantage of 1D-FGM, a new type of FGM is needed whose material properties can vary in two or three directions. For this reason, there are many studies in the literature examining the mechanical behavior of two-directional functionally graded beams (2D-FGBs) with numerical and analytical methods according to various beam theories. Among the studies carried out with the finite element method, which is the most widely used numerical method in the literature, we can mention the following: Karamanlı and Vo [19] performed the size-dependent bending analysis of two-directional functionally graded microbeams via a quasi-3D theory and finite element method. Chinh et al.

M. Turan (✉)

Department of Civil Engineering, Faculty of Engineering, Bayburt University, 69010 Bayburt, Turkey
e-mail: mturan@bayburt.edu.tr

[20] investigated the elastostatic bending behavior of a two-directional functionally graded sandwich beam under various types of non-uniform distributed loads by a finite element model. Chen et al. [21] presented nonlinear free vibration analysis of a rotating two-directional functionally graded porous micro-beam using isogeometric analysis based on the Timoshenko beam theory. Nguyen et al. [22] investigated the dynamic behavior of a two-directional functionally graded sandwich beam made of three different materials due to the non-uniform motion of a moving point load. Viet et al. [23] presented free vibration analysis based on a finite element model of unidirectional and bidirectional functionally graded cantilever beams. Le et al. [24] proposed an efficient third-order shear deformation beam element for free vibration and buckling analysis of two-directional functionally graded sandwich beams.

Among analytical works, we can mention the following: Lü et al. [25] presented elasticity solutions for bending and thermal deformations of bi-directional FGBs with different end conditions, using the state space-based differential quadrature method. Şimşek [26] investigated free and forced vibration of bi-directional functionally graded Timoshenko beam under the action of a moving load. Şimşek [27] studied buckling of Timoshenko beams composed of 2D-FGBs having different boundary conditions. Nejad et al. [28] presented buckling analysis of arbitrary two-directional functionally graded Euler–Bernoulli nano-beams based on non-local elasticity theory. Wang et al. [29] proposed an analytical solution for free vibration of a functionally graded beam with variable material properties along the beam length and thickness. Karamanlı [30–32] presented the bending and elastostatic behavior of 2D-FGBs subjected to various sets of boundary conditions by using different shear deformation theories and the Symmetric Smoothed Particle Hydrodynamics method. Karamanlı [33–35] investigated free vibration and buckling of 2D-FGBs according to different beam theories using various solution methods. Shanab and Attia [36] studied semi-analytical solutions for static and dynamic responses of bi-directional functionally graded non-uniform nanobeams with surface energy effects. Huang [37] investigated bending and free vibration behaviors of bi-directional functionally graded cylindrical beams. Huang and Ouyang [38] presented the exact solution for bending analysis of 2D-FG Timoshenko beams.

Although there are many studies dealing with the mechanical behavior of FGM beams by numerical and analytical methods, the literature review shows that research on 2D-FGBs with employing Navier’s method is limited. The most critical situation that distinguishes the existing studies for Navier’s method is the functions used in the solution. In this method, trigonometric functions that satisfy the boundary conditions for the solution should be selected. Due to the difficulty in selecting these functions, studies using Navier’s method have generally been limited to simple beams. By the literature survey and authors’ knowledge, there is no study examining the bending behavior of 2D-FGBs with the proposed trigonometric series functions. This study aims to perform a bending analysis of 2D-FGBs with various boundary conditions using trigonometric series functions and to investigate the accuracy of the trigonometric series functions. The difference between Huang and Ouyang [38] used for comparison and the presented study is methods. They used the equilibrium equations for the plane state of elasticity in their research. Proposed trigonometric series functions were used before by Nguyen et al. [39] for static, vibration, and buckling of laminated composite beams. The governing equations are derived according to Lagrange’s principle. A power-law rule defines the variation of the components of the beam material in the volume. The normalized maximum transverse deflections, the normalized axial, and transverse shear stresses are obtained for various boundary conditions, gradation exponents (p_x, p_z) in the x - and z -directions, and the slenderness (L/h). In addition, this study aims to present some benchmark results for the bending behavior of 2D-FGBs subjected to various sets of boundary conditions with employing Navier’s method. Some new graphs that can be used as reference data for the future are presented in parametric studies.

2 Theory and formulation

2.1 Material properties

Figure 1 shows a two-directional functionally graded beam of length L , width b , thickness h . The x -, y -, and z -axes are located along the length, width, and thickness of the beam, respectively. The beam is subjected to a uniformly distributed loading q_0 in the same direction as the z -axis. The beam consists of a mixture of two components such as ceramic (Al_2O_3) and metal (Al). According to the rule of mixtures, the effective material properties can be given by

$$P(x, z) = P_c V_c(x, z) + P_m V_m(x, z) \quad (1)$$

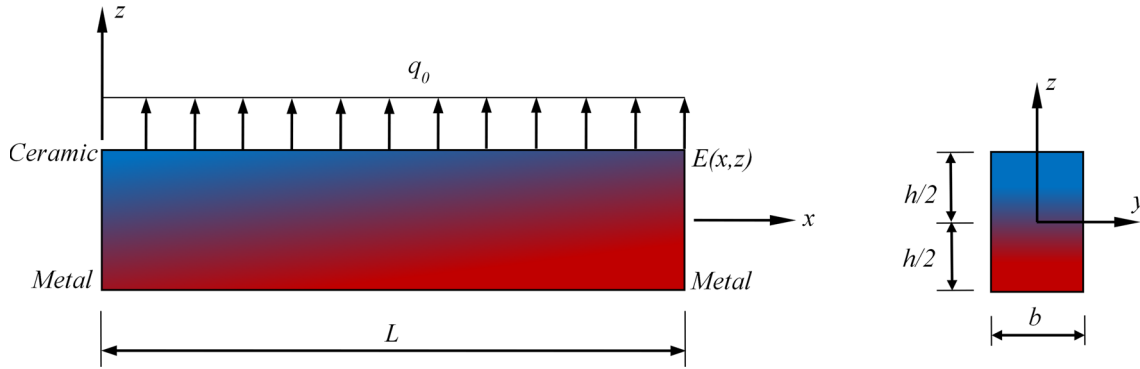


Fig. 1 Geometry of a 2D-FGBs under uniformly distributed loading with the corresponding coordinates

where P_m and P_c are the corresponding material properties of the metal and ceramic constituents, e.g., Young’s modulus E , Poisson’s ratio ν , and mass density ρ , respectively. V_c and V_m are the volume fractions of the ceramic and metal, and they are related by

$$V_c(x, z) + V_m(x, z) = 1 \tag{2}$$

For the 2D-FGBs, the effective material properties are assumed to follow the power-law rule. The volume fraction of ceramic constituent is defined by

$$V_c(x, z) = \left(1 - \frac{x}{2L}\right)^{p_x} \left(\frac{1}{2} + \frac{z}{h}\right)^{p_z} \tag{3}$$

where p_x , and p_z are the gradation exponents (power-law exponents) in the x and z directions. The variation of the volume fraction (V_c) in two dimensions is shown in Fig. 2.

Using Eqs. (1, 2 and 3), the effective material properties of the 2D-FGB whose material properties vary continuously through the length and thickness can be found as follows:

$$P(x, z) = (P_c - P_m) \left(1 - \frac{x}{2L}\right)^{p_x} \left(\frac{1}{2} + \frac{z}{h}\right)^{p_z} + P_m \tag{4}$$

Based on Eq. (4), one can be expressed for the Young’s modulus E and shear modulus G by

$$\begin{aligned} E(x, z) &= (E_c - E_m) \left(1 - \frac{x}{2L}\right)^{p_x} \left(\frac{1}{2} + \frac{z}{h}\right)^{p_z} + E_m \\ G(x, z) &= (G_c - G_m) \left(1 - \frac{x}{2L}\right)^{p_x} \left(\frac{1}{2} + \frac{z}{h}\right)^{p_z} + G_m \end{aligned} \tag{5}$$

where E_m, E_c , and G_m, G_c are Young’s modulus and shear modulus of metal and ceramic, respectively.

2.2 Governing Equations and Analytical Solution

The nonzero components of the displacement field of FSDT are given by

$$\begin{aligned} u(x, z, t) &= u^0(x, t) + z \phi^0(x, t), \\ w(x, z, t) &= w^0(x, t) \end{aligned} \tag{6}$$

Here superscript “0” indicates the variable at the neutral axis. According to the geometrical and physical linearity assumptions, the strain–displacement relations and stresses of the beam take the following form:

$$\varepsilon_{xx} = \frac{\partial u}{\partial x} = u_{,x}^0 + z \phi_{,x}^0, \quad \gamma_{xz} = \frac{\partial u}{\partial z} + \frac{\partial w}{\partial x} = w_{,x}^0 + \phi^0 \tag{7}$$

$$\sigma_{xx} = E(x, z) \varepsilon_{xx}, \quad \tau_{xz} = K G(x, z) \gamma_{xz} \tag{8}$$

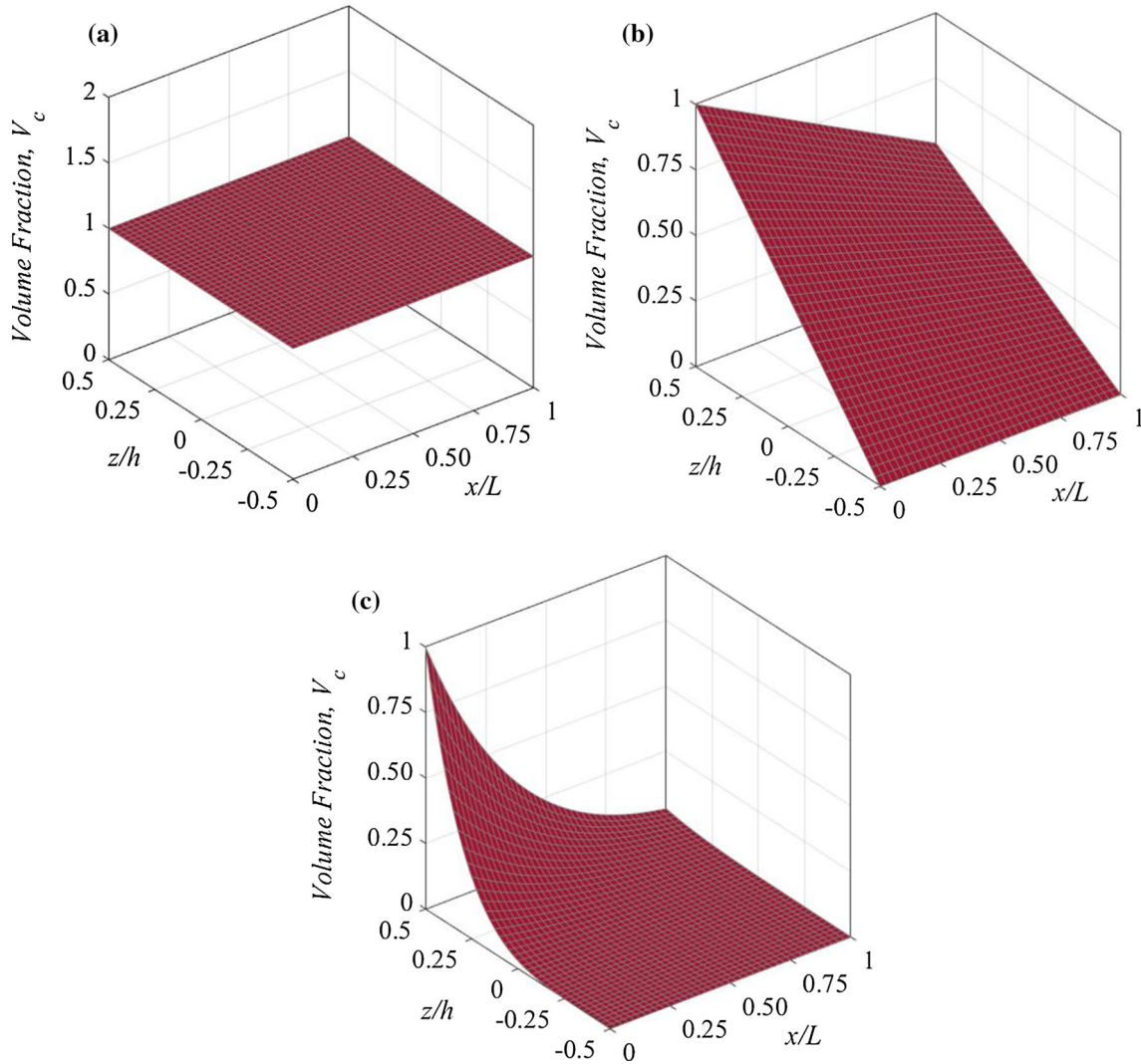


Fig. 2 Variation of the volume fraction (V_c) in x and z directions for a) $p_x = p_z = 0$, b) $p_x = p_z = 1$, c) $p_x = p_z = 5$

where ε_{xx} is the normal strain, γ_{xz} is the shear strains, σ_{xx} is the normal stress, τ_{xz} is the shear stress, K is the shear correction factor, $E(x, z)$ is the Young modulus, and $G(x, z)$ is the shear modulus. $(\cdot)_{,x}$ denotes the derivative with respect to x .

The governing equations can be obtained by Lagrange’s equations given by

$$\frac{d}{dt} \left(\frac{\partial \Pi}{\partial \dot{q}_i} \right) - \frac{\partial \Pi}{\partial q_i} = 0 \tag{9}$$

where q_i represents the variables of u_i , w_i and ϕ_i . The Lagrangian functional is expressed in the following form

$$\Pi = T - (U + V) \tag{10}$$

The strain energy of the beam can be expressed by

$$U = \frac{1}{2} \int_0^L \int_A (\sigma_{xx} \varepsilon_{xx} + \tau_{xz} \gamma_{xz}) dA dx \tag{11}$$

where A is the cross-sectional area of the beam. If Eqs. (7) and (8) are substituted into Eq. (11) together with Eq. (5), one can obtain the strain energy in the following form

$$U = \frac{1}{2} \int_0^L \left\{ (u_{,x}^0)^2 \left[A_0 \left(1 - \frac{x}{2L} \right)^{p_x} + A_1 \right] + 2u_{,x}^0 \phi_{,x}^0 \left[B_0 \left(1 - \frac{x}{2L} \right)^{p_x} + B_1 \right] + (\phi_{,x}^0)^2 \left[C_0 \left(1 - \frac{x}{2L} \right)^{p_x} + C_1 \right] + (w_{,x}^0 + \phi^0)^2 \left[D_0 \left(1 - \frac{x}{2L} \right)^{p_x} + D_1 \right] \right\} dx \tag{12}$$

where the stiffness coefficients are defined as

$$\begin{aligned} &= b \int_{-h/2}^{h/2} (E_c - E_m) \left(\frac{1}{2} + \frac{z}{h} \right)^{p_z} [1, z, z^2] dz, \quad [A_1, B_1, C_1] = b \int_{-h/2}^{h/2} E_m [1, z, z^2] dz \\ D_0 &= b \int_{-h/2}^{h/2} K (G_c - G_m) \left(\frac{1}{2} + \frac{z}{h} \right)^{p_z} dz, \quad D_1 = b \int_{-h/2}^{h/2} K G_m dz \end{aligned} \tag{13}$$

The kinetic energy of beam can be given by

$$T = \frac{1}{2} \int_0^{L_e} \int_A \rho(x, z) (\dot{u}^2 + \dot{w}^2) dA dx \tag{14}$$

where dot denotes the derivative with respect to time. Taking the derivative of Eqs. (6) with respect to time, and substituting the result into Eq. (14) gives in the following form

$$T = \frac{1}{2} \int_0^L \left\{ (\dot{u}^0)^2 \left[I_0 \left(1 - \frac{x}{2L} \right)^{p_x} + I_{00} \right] + 2\dot{u}^0 \dot{\phi}^0 \left[I_1 \left(1 - \frac{x}{2L} \right)^{p_x} + I_{11} \right] + (\dot{\phi}^0)^2 \left[I_2 \left(1 - \frac{x}{2L} \right)^{p_x} + I_{22} \right] + (\dot{w}^0)^2 \left[I_0 \left(1 - \frac{x}{2L} \right)^{p_x} + I_{00} \right] \right\} dx \tag{15}$$

where the inertia coefficients are

$$[I_0, I_1, I_2] = b \int_{-h/2}^{h/2} (\rho_c - \rho_m) \left(\frac{1}{2} + \frac{z}{h} \right)^{p_z} [1, z, z^2] dz, \quad [I_{00}, I_{11}, I_{22}] = b \int_{-h/2}^{h/2} \rho_m [1, z, z^2] dz \tag{16}$$

where ρ_m and ρ_c are the mass density of metal and ceramic, respectively. The work done by the vertical uniformly distributed loading q_0 can be expressed as

$$V = \int_0^L q_0 w^0 dx \tag{17}$$

Solutions to $u^0(x, t)$, $w^0(x, t)$ and $\phi^0(x, t)$ can be assumed as

$$u^0(x, t) = \sum_{i=1}^m \varphi_i(x) u_i(t), \quad w^0(x, t) = \sum_{i=1}^m \psi_i(x) w_i(t), \quad \phi^0(x, t) = \sum_{i=1}^m \theta_i(x) \phi_i(t) \tag{18}$$

where $\varphi_i(x)$, $\psi_i(x)$ and $\theta_i(x)$ are trigonometric series functions that change depending on the boundary conditions of the beam, and $u_i(t)$, $w_i(t)$ and $\phi_i(t)$ are the generalized nodal displacements, and m represents the number of trigonometric series. The trigonometric series functions selected to satisfy the boundary conditions for the beams considered in the study are given in Table 1. Here, SS refers to the simply supported beam, CC to the clamped–clamped beam, and CF to the clamped-free beam.

Substituting Eqs. (12), (15) and (17) into Eq. (9) with considering Eqs. (18) leads to

$$\begin{bmatrix} \mathbf{m}^{11} & \mathbf{0} & \mathbf{m}^{13} \\ \mathbf{0} & \mathbf{m}^{22} & \mathbf{0} \\ \mathbf{m}^{13T} & \mathbf{0} & \mathbf{m}^{33} \end{bmatrix} \begin{Bmatrix} \ddot{u}_i \\ \ddot{w}_i \\ \ddot{\phi}_i \end{Bmatrix} + \begin{bmatrix} \mathbf{k}^{11} & \mathbf{0} & \mathbf{k}^{13} \\ \mathbf{0} & \mathbf{k}^{22} & \mathbf{k}^{23} \\ \mathbf{k}^{13T} & \mathbf{k}^{23T} & \mathbf{k}^{33} \end{bmatrix} \begin{Bmatrix} u_i \\ w_i \\ \phi_i \end{Bmatrix} = \begin{Bmatrix} 0 \\ \mathbf{f}_2 \\ 0 \end{Bmatrix} \tag{19}$$

where \mathbf{m} , \mathbf{k} and \mathbf{f} are the mass matrix, the stiffness matrix and the force vector, respectively. \mathbf{m} , \mathbf{k} and \mathbf{f}_2 are explicitly expressed for SS 2D-FGB in the following form

Table 1 Kinematic boundary conditions and trigonometric series functions used in Navier’s method

BCs	$\varphi_i(x)$	$\psi_i(x)$	$\theta_i(x)$	$x = 0$	$x = L$
SS	$\cos \frac{i\pi x}{L}$	$\sin \frac{i\pi x}{L}$	$\cos \frac{i\pi x}{L}$	$w^0 = 0$	$w^0 = 0$
CC	$\sin \frac{2i\pi x}{L}$	$\sin^2 \frac{i\pi x}{L}$	$\sin \frac{2i\pi x}{L}$	$u^0 = w^0 = \phi^0 = w_{,x}^0 = 0$	$u^0 = w^0 = \phi^0 = w_{,x}^0 = 0$
CF	$\sin \frac{(2i-1)\pi x}{2L}$	$1 - \cos \frac{(2i-1)\pi x}{2L}$	$\sin \frac{(2i-1)\pi x}{2L}$	$u^0 = w^0 = \phi^0 = w_{,x}^0 = 0$	

$$\begin{aligned}
 \mathbf{m}_{ij}^{11} &= \int_0^L \left\{ I_0 \left(1 - \frac{x}{2L} \right)^{p_x} + I_{00} \right\} \cos \left(\frac{i\pi}{L} x \right) \cos \left(\frac{j\pi}{L} x \right) dx, \\
 \mathbf{m}_{ij}^{13} &= \int_0^L \left\{ I_1 \left(1 - \frac{x}{2L} \right)^{p_x} + I_{11} \right\} \cos \left(\frac{i\pi}{L} x \right) \cos \left(\frac{j\pi}{L} x \right) dx, \\
 \mathbf{m}_{ij}^{22} &= \int_0^L \left\{ I_0 \left(1 - \frac{x}{2L} \right)^{p_x} + I_{00} \right\} \sin \left(\frac{i\pi}{L} x \right) \sin \left(\frac{j\pi}{L} x \right) dx, \\
 \mathbf{m}_{ij}^{33} &= \int_0^L \left\{ I_2 \left(1 - \frac{x}{2L} \right)^{p_x} + I_{22} \right\} \cos \left(\frac{i\pi}{L} x \right) \cos \left(\frac{j\pi}{L} x \right) dx, \\
 \mathbf{k}_{ij}^{11} &= \int_0^L ij \frac{\pi^2}{L^2} \left\{ A_0 \left(1 - \frac{x}{2L} \right)^{p_x} + A_1 \right\} \sin \left(\frac{i\pi}{L} x \right) \sin \left(\frac{j\pi}{L} x \right) dx, \\
 \mathbf{k}_{ij}^{13} &= \int_0^L ij \frac{\pi^2}{L^2} \left\{ B_0 \left(1 - \frac{x}{2L} \right)^{p_x} + B_1 \right\} \sin \left(\frac{i\pi}{L} x \right) \sin \left(\frac{j\pi}{L} x \right) dx, \\
 \mathbf{k}_{ij}^{22} &= \int_0^L ij \frac{\pi^2}{L^2} \left\{ D_0 \left(1 - \frac{x}{2L} \right)^{p_x} + D_1 \right\} \cos \left(\frac{i\pi}{L} x \right) \cos \left(\frac{j\pi}{L} x \right) dx, \\
 \mathbf{k}_{ij}^{23} &= \int_0^L i \frac{\pi}{L} \left\{ D_0 \left(1 - \frac{x}{2L} \right)^{p_x} + D_1 \right\} \cos \left(\frac{i\pi}{L} x \right) \cos \left(\frac{j\pi}{L} x \right) dx, \\
 \mathbf{k}_{ij}^{33} &= \int_0^L ij \frac{\pi^2}{L^2} \left\{ C_0 \left(1 - \frac{x}{2L} \right)^{p_x} + C_1 \right\} \sin \left(\frac{i\pi}{L} x \right) \sin \left(\frac{j\pi}{L} x \right) dx \\
 &\quad + \int_0^L \left\{ D_0 \left(1 - \frac{x}{2L} \right)^{p_x} + D_1 \right\} \cos \left(\frac{i\pi}{L} x \right) \cos \left(\frac{j\pi}{L} x \right) dx, \\
 \mathbf{f}_2 &= \frac{Lq_0}{i\pi} [1 - \cos(i\pi)] \quad \text{with } i = j = 1, 2, \dots, m
 \end{aligned} \tag{20}$$

The matrix governing equation of the 2D-FGB with the length of L in terms of \mathbf{U} can be written as follows

$$\mathbf{M}\ddot{\mathbf{U}} + \mathbf{K}\mathbf{U} = \mathbf{F} \tag{21}$$

where \mathbf{M} , \mathbf{K} and \mathbf{F} are the mass, stiffness matrix and the force vector, respectively. \mathbf{U} is the vector of unknowns, and is as follows

$$\mathbf{U} = \{u_1 \ \cdots \ u_m \ w_1 \ \cdots \ w_m \ \phi_1 \ \cdots \ \phi_m\}^T \tag{22}$$

Table 2 Convergence studies for normalized maximum transverse deflections of the 2D-FGBs with the different boundary conditions ($u^0 \neq 0, L/h = 5, p_x = p_z = 2$)

Number of trigonometric series, m	SS	CC	CF
1	9.9652	2.4536	78.4899
3	10.0019	2.5415	80.0493
5	10.0083	2.5699	80.2224
7	10.0067	2.5838	80.2862
8	10.0062	2.5836	80.3056
10	10.0077	2.5920	80.3315
12	10.0069	2.5975	80.3485
14	10.0074	2.6014	80.3606
16	10.0071	2.6044	80.3696
18	10.0073	2.6067	80.3766
Exact [38]	10.02139	2.681505	80.43270

For bending analysis, \mathbf{M} is zero ($\mathbf{M} = \mathbf{0}$) in Eq. (21). The system equations given by Eq. (21) has been solved numerically by using any numerical method. After this process, displacements and stresses are calculated.

3 Results and discussion

In this section, some numerical results obtained from the bending analysis of 2D-FGBs with various boundary conditions are presented. Numerical results are obtained with a code written in the MATLAB [40] program. The accuracy of the proposed trigonometric series functions for each boundary condition is investigated. In addition, some new graphs that can be used as reference data for the future are presented as parametric studies. The physical parameters of the beam are $L = 1$ m and $b = 0.1$ m. Two different slenderness such that $L/h = 5$ and 20 are considered. The uniformly distributed loading q_0 is $10,000$ N/m. The shear correction factor is considered to be $K = 5/6$ for rectangular cross sections. A functionally graded beam composed of aluminum (Al) as metal and alumina (Al_2O_3) as ceramic is considered for which $E_m = 70$ GPa, $\rho_m = 2702$ kg/m³, $\nu_m = 0.3$, $E_c = 380$ GPa, $\rho_c = 3960$ kg/m³, and $\nu_c = 0.3$. The transverse deflections, axial and shear stresses are given in the following normalized form:

$$\bar{w} = \frac{100E_m b h^3}{q_0 L^4} w(x, 0), \quad \bar{\sigma}_{xx} = \frac{bh}{q_0 L} \sigma_{xx}(x, z), \quad \bar{\tau}_{xz} = \frac{bh}{q_0 L} \tau_{xz}(x, z) \quad (23)$$

3.1 Convergence study

A convergence study is performed to determine the number of trigonometric series that will be sufficient. The normalized maximum transverse deflections of the 2D-FGBs with respect to the number of trigonometric series m for different boundary conditions ($u^0 \neq 0, L/h = 5, p_x = p_z = 2$) are given in Table 2. It is observed that the deflections converge quickly for three boundary conditions. Fourteen trigonometric series ($m = 14$) seem to be enough for the desired accuracy in numerical calculations. In addition, the results of the proposed solution agree well with the exact solution given by Ref. [38].

3.2 Verification with previous results

Verification studies are carried out to demonstrate the accuracy of the proposed solution and to investigate the responses of 2D-FGBs with various boundary conditions for bending problems. Tables 3 and 4 show a comparison of the normalized maximum transverse deflections of the SS 2D-FGBs for various slenderness ($L/h = 5, L/h = 20$) and gradation exponents. For $u^0 = 0$, the effects of longitudinal displacements are neglected. For $u^0 \neq 0$, it is not neglected. The tables compare the normalized maximum transverse deflections of the SS 2D-FGBs with the results of Huang and Ouyang [38], which is the exact solution based on the Timoshenko beam theory. The results are in good agreement as seen. According to these tables, the smallest normalized displacements occur when $p_x = p_z = 0$ (fully ceramic) for $L/h = 5$ and 20 . With the increase of the p_x and p_z in both directions, the transverse deflections increase. The normalized maximum transverse deflection decreases

Table 3 Comparison of the normalized maximum transverse deflections of the SS 2D-FGBs for various gradation exponents, $L/h = 5$

	$p_x = 0$		$p_x = 0.5$		$p_x = 1$		$p_x = 2$		$p_x = 5$	
	Present	[38]	Present	[38]	Present	[38]	Present	[38]	Present	[38]
$u^0 = 0$										
$p_z = 0$	3.1657	3.165658	3.5696	3.570196	4.0155	4.018162	5.0247	5.035384	8.5094	8.543177
$p_z = 0.5$	4.5244	4.524283	5.0379	5.038563	5.5875	5.590249	6.7665	6.77707	10.2858	10.31679
$p_z = 1$	5.3465	5.346444	5.9091	5.909761	6.5000	6.50278	7.7310	7.74031	11.1523	11.17526
$p_z = 2$	6.2680	6.267887	6.8699	6.870436	7.4896	7.49151	8.7407	8.7464	11.9905	11.99889
$p_z = 5$	7.7952	7.795057	8.4253	8.425339	9.0538	9.053855	10.2672	10.26585	13.1446	13.13675
$u^0 \neq 0$										
$p_z = 0$	3.1657	3.165658	3.5696	3.570196	4.0155	4.018162	5.0247	5.035384	8.5094	8.543177
$p_z = 0.5$	4.8349	4.834847	5.3544	5.355052	5.9045	5.90771	7.0688	7.081084	10.4737	10.5115
$p_z = 1$	6.2600	6.259923	6.8082	6.809204	7.3702	7.374088	8.5064	8.520527	11.5713	11.60851
$p_z = 2$	8.0304	8.030299	8.5274	8.528547	9.0252	9.029599	10.0074	10.02139	12.5844	12.6109
$p_z = 5$	9.6485	9.648317	10.0798	10.080426	10.5147	10.51725	11.3769	11.38281	13.5941	13.59786

Table 4 Comparison of the normalized maximum transverse deflections of the SS 2D-FGBs for various gradation exponents, $L/h = 20$

	$p_x = 0$		$p_x = 0.5$		$p_x = 1$		$p_x = 2$		$p_x = 5$	
	Present	[38]	Present	[38]	Present	[38]	Present	[38]	Present	[38]
$u^0 = 0$										
$p_z = 0$	2.8963	2.89625	3.2641	3.26322	3.6717	3.668114	4.6004	4.585229	7.8653	7.791128
$p_z = 0.5$	4.1543	4.154253	4.6231	4.622164	5.1266	5.122814	6.2140	6.199182	9.5121	9.457342
$p_z = 1$	4.8915	4.891444	5.4039	5.402989	5.9447	5.940865	7.0791	7.065215	10.2861	10.2409
$p_z = 2$	5.6773	5.677262	6.2239	6.223043	6.7902	6.786574	7.9446	7.931764	10.9996	10.96334
$p_z = 5$	6.9536	6.953618	7.5296	7.528709	8.1090	8.105773	9.2406	9.229903	11.9757	11.94989
$u^0 \neq 0$										
$p_z = 0$	2.8963	2.89625	3.2641	3.26322	3.6717	3.668114	4.6004	4.585229	7.8653	7.791128
$p_z = 0.5$	4.4648	4.464817	4.9395	4.938653	5.4438	5.440275	6.5166	6.503195	9.7009	9.652053
$p_z = 1$	5.8049	5.804923	6.3031	6.302432	6.8149	6.812172	7.8553	7.845432	10.7071	10.67415
$p_z = 2$	7.4397	7.439674	7.8816	7.881153	8.3262	8.324664	9.2125	9.206755	11.5963	11.57536
$p_z = 5$	8.8069	8.806879	9.1840	9.183795	9.5700	9.569164	10.3510	10.34686	12.4264	12.41100

as the L/h increases. For $p_z = 0$, the normalized maximum transverse deflections do not change according to the results of $u^0 = 0$ and $u^0 \neq 0$. For $p_z \neq 0$, the results of $u^0 = 0$ are smaller than the other.

In Tables 5 and 6, the normalized axial and transverse shear stresses of the SS 2D-FGBs are given for $u^0 \neq 0$. There is no difference in mechanical behavior between the $u^0 = 0$ and $u^0 \neq 0$. The results of this study are compared with those of Karamanlı [32] based on a four-unknown shear and normal deformation theory and Vo et al. [6] based on FSDT for $p_x = 0$. The results for axial stresses are in good agreement. For transverse shear stresses, the results do not agree with those of Karamanlı [32] because the theories are different, but they are in good agreement with those of Vo et al. [6]. The transverse shear strain is assumed to be constant in the beam depth direction in the FSDT. In higher-order shear deformation theories, the transverse shear strain is not constant throughout the depth. It is clear that the axial stress decreases as the gradation exponent in the x -direction increases for $p_z \neq 0$. In the z -direction, they increase with increasing p_z . The transverse shear stresses increase with the increase of p_x . They decrease with the increase of p_z .

Comparison of the normalized maximum transverse deflections of the CC 2D-FGBs for various gradation exponents and the slenderness ($L/h = 5, L/h = 20$) is given in Tables 7 and 8. The results are in good agreement with those of Ref. [38]. It is clear that the deflections increase as the gradation exponents increase.

Verification of the normalized maximum transverse deflections of the CF 2D-FGBs for various gradation exponents and the slenderness is shown in Tables 9 and 10. Here, a good agreement is observed between the results. Also, as it is expected, the largest deflections occur in the CF beam within the considered boundary conditions. As it is seen from Tables 9 and 10, the transverse deflections increase as the p_x and p_z increase due to the lower stiffness.

Table 5 The normalized axial stress $\bar{\sigma}_{xx}(L/2, h/2)$ of the SS 2D-FGBs ($u^0 \neq 0$)

	$p_x = 0$			$p_x = 1$		$p_x = 2$		$p_x = 5$	
	Present	[32]	[6]	Present	[32]	Present	[32]	Present	[32]
<i>L/h = 5</i>									
$p_z = 0$	3.7507	3.8005	3.7500	3.7509	3.7945	3.7511	3.7703	3.7508	3.6740
$p_z = 1$	5.7969	5.8815	5.7959	5.5445	5.6196	5.2965	5.3454	4.6474	4.6207
$p_z = 2$	6.7689	6.8821	6.7676	6.3154	6.4155	5.9072	5.9789	4.9507	4.9475
$p_z = 5$	7.9442	8.1145	7.9428	7.3363	7.4802	6.7858	6.8933	5.4535	5.4784
<i>L/h = 20</i>									
$p_z = 0$	15.0027	15.0147	15.0000	15.0036	14.9895	15.0045	14.8909	15.0033	14.5014
$p_z = 1$	23.1877	23.2099	23.1834	22.1780	22.1731	21.1858	21.0861	18.5895	18.2136
$p_z = 2$	27.0754	27.1122	27.0704	25.2618	25.2728	23.6288	23.5505	19.8028	19.4770
$p_z = 5$	31.7769	31.8070	31.7711	29.3452	29.3394	27.1433	27.0385	21.8141	21.5344

Table 6 The normalized transverse shear stress $\bar{\sigma}_{xz}(0, 0)$ of the SS 2D-FGBs ($u^0 \neq 0$)

	$p_x = 0$			$p_x = 1$		$p_x = 2$		$p_x = 5$	
	Present	[32]	[6]	Present	[32]	Present	[32]	Present	[32]
<i>L/h = 5</i>									
$p_z = 0$	0.5827	0.7246	0.5976	0.6383	0.7923	0.6842	0.8484	0.7502	0.9278
$p_z = 1$	0.5827	0.7234	0.5976	0.6276	0.7780	0.6614	0.8186	0.7031	0.8662
$p_z = 2$	0.4958	0.6618	0.5085	0.5280	0.7017	0.5508	0.7290	0.5768	0.7582
$p_z = 5$	0.3816	0.5840	0.3914	0.3984	0.6001	0.4092	0.6099	0.4205	0.6203
<i>L/h = 20</i>									
$p_z = 0$	0.5827	0.7425	0.5976	0.6383	0.8125	0.6842	0.8718	0.7502	0.9580
$p_z = 1$	0.5827	0.7432	0.5976	0.6276	0.7993	0.6614	0.8415	0.7031	0.8901
$p_z = 2$	0.4958	0.6789	0.5085	0.5280	0.7199	0.5508	0.7486	0.5768	0.7792
$p_z = 5$	0.3816	0.6037	0.3914	0.3984	0.6223	0.4092	0.6364	0.4205	0.6385

Table 7 Comparison of the normalized maximum transverse deflections of the CC 2D-FGBs for various gradation exponents, $L/h = 5$

	$p_x = 0$		$p_x = 0.5$		$p_x = 1$		$p_x = 2$		$p_x = 5$	
	Present	[38]	Present	[38]	Present	[38]	Present	[38]	Present	[38]
<i>u⁰ = 0</i>										
$p_z = 0$	0.8547	0.863026	0.9647	0.978111	1.0737	1.10022	1.2816	1.356669	1.9214	2.049671
$p_z = 0.5$	1.2092	1.220616	1.3486	1.365809	1.4833	1.514758	1.7319	1.810773	2.4582	2.516059
$p_z = 1$	1.4435	1.457556	1.5973	1.617412	1.7438	1.777834	2.0083	2.085985	2.7100	2.771532
$p_z = 2$	1.7393	1.757577	1.9056	1.929766	2.0609	2.097836	2.3341	2.407925	2.9803	3.049694
$p_z = 5$	2.2510	2.277039	2.4229	2.453877	2.5784	2.619059	2.8412	2.906739	3.4041	3.449993
<i>u⁰ ≠ 0</i>										
$p_z = 0$	0.8547	0.863026	0.9647	0.978111	1.0737	1.10022	1.2816	1.356669	1.9214	2.049671
$p_z = 0.5$	1.2713	1.282729	1.4119	1.429198	1.5471	1.578524	1.7945	1.873337	2.5143	2.571593
$p_z = 1$	1.6262	1.640251	1.7773	1.797394	1.9191	1.953105	2.1707	2.249226	2.8374	2.905973
$p_z = 2$	2.0918	2.11006	2.2369	2.261353	2.3703	2.408455	2.6014	2.681505	3.1623	3.259906
$p_z = 5$	2.6216	2.647691	2.7529	2.784842	2.8723	2.916499	3.0761	3.154211	3.5429	3.627800

3.3 Parametric study

This section presents the normalized transverse deflections, axial and shear stresses of 2D-FGBs with various boundary conditions. Since there is no difference in mechanical behavior between neglecting and not ignoring the effects of longitudinal displacements, results are given according to $u^0 \neq 0$. The beams have the slenderness $L/h = 5$.

Normalized transverse deflections of the SS 2D-FGBs with respect to the normalized coordinate x/L for various gradation exponents are presented in Fig. 3. As can be seen from the figure, it is clear that the transverse deflections increase with the increase in the gradation exponent (i.e., the metallic character of the beam increases). The location of the normalized maximum transverse deflections of the SS 2D-FGBs is at or

Table 8 Comparison of the normalized maximum transverse deflections of the CC 2D-FGBs for various gradation exponents, $L/h = 20$

	$p_x = 0$		$p_x = 0.5$		$p_x = 1$		$p_x = 2$		$p_x = 5$	
	Present	[38]	Present	[38]	Present	[38]	Present	[38]	Present	[38]
$u^0 = 0$										
$p_z = 0$	0.5931	0.593618	0.6694	0.672502	0.7450	0.755911	0.8896	0.930423	1.3350	1.403893
$p_z = 0.5$	0.8498	0.850586	0.9473	0.950911	1.0415	1.053375	1.2153	1.255979	1.7227	1.738709
$p_z = 1$	1.0016	1.002556	1.1083	1.112183	1.2100	1.221954	1.3940	1.432535	1.8825	1.90403
$p_z = 2$	1.1657	1.166952	1.2798	1.283877	1.3869	1.398537	1.5765	1.611873	2.0286	2.062482
$p_z = 5$	1.4339	1.4356	1.5541	1.558375	1.6643	1.674906	1.8531	1.882173	2.2636	2.286525
$u^0 \neq 0$										
$p_z = 0$	0.5931	0.593618	0.6694	0.672502	0.7450	0.755911	0.8896	0.930423	1.3350	1.403893
$p_z = 0.5$	0.9119	0.912698	1.0106	1.014243	1.1052	1.116901	1.2779	1.317594	1.7787	1.791193
$p_z = 1$	1.1843	1.185251	1.2883	1.291978	1.3853	1.396487	1.5563	1.593176	2.0099	2.031677
$p_z = 2$	1.5182	1.519435	1.6112	1.615071	1.6963	1.70773	1.8438	1.881155	2.2105	2.264002
$p_z = 5$	1.8045	1.806252	1.8842	1.888996	1.9581	1.971252	2.0880	2.126988	2.4024	2.460596

Table 9 Comparison of the normalized maximum transverse deflections of the CF 2D-FGBs for various gradation exponents, $L/h = 5$

	$p_x = 0$		$p_x = 0.5$		$p_x = 1$		$p_x = 2$		$p_x = 5$	
	Present	[38]	Present	[38]	Present	[38]	Present	[38]	Present	[38]
$u^0 = 0$										
$p_z = 0$	28.7473	28.78105	30.1186	30.15195	31.5755	31.60848	34.7396	34.77199	45.7295	45.76062
$p_z = 0.5$	41.1764	41.22281	42.9325	42.97844	44.7654	44.81086	48.6286	48.67326	60.9351	60.97813
$p_z = 1$	48.5509	48.60800	50.4807	50.53714	52.4738	52.52971	56.6042	56.65927	69.1962	69.24943
$p_z = 2$	56.5698	56.64371	58.6409	58.71418	60.7554	60.82806	65.0592	65.13087	77.6258	77.69539
$p_z = 5$	69.7012	69.80635	71.8873	71.99178	74.0785	74.18235	78.4199	78.52272	90.3718	90.47245
$u^0 \neq 0$										
$p_z = 0$	28.7473	28.78105	30.1186	30.15195	31.5755	31.60848	34.7396	34.77199	45.7295	45.76062
$p_z = 0.5$	44.1577	44.20422	45.9387	45.98466	47.7866	47.83211	51.6488	51.69343	63.7482	63.79118
$p_z = 1$	57.3202	57.37739	59.2108	59.26747	61.1355	61.19166	65.0491	65.10426	76.6154	76.66856
$p_z = 2$	73.4886	73.56287	75.2007	75.27434	76.9204	76.99351	80.3606	80.4327	90.2656	90.33556
$p_z = 5$	87.4922	87.59765	88.9659	89.07082	90.4545	90.5589	93.4475	93.55095	102.0546	102.1562

Table 10 Comparison of the normalized maximum transverse deflections of the CF 2D-FGBs for various gradation exponents, $L/h = 20$

	$p_x = 0$		$p_x = 0.5$		$p_x = 1$		$p_x = 2$		$p_x = 5$	
	Present	[38]	Present	[38]	Present	[38]	Present	[38]	Present	[38]
$u^0 = 0$										
$p_z = 0$	27.7008	27.70342	28.9828	28.98523	30.3420	30.34430	33.2873	33.28938	43.5259	43.52787
$p_z = 0.5$	39.7390	39.74269	41.3841	41.38755	43.0985	43.10171	46.7071	46.71000	58.2329	58.2355
$p_z = 1$	46.7836	46.78800	48.5885	48.59271	50.4511	50.45505	54.3100	54.31365	66.1305	66.13375
$p_z = 2$	54.2756	54.28121	56.2086	56.21395	58.1829	58.18802	62.2083	62.21300	74.0573	74.06156
$p_z = 5$	66.4328	66.4406	68.4824	68.48991	70.5421	70.54933	74.6405	74.64726	86.0439	86.05008
$u^0 \neq 0$										
$p_z = 0$	27.7008	27.70342	28.9828	28.98523	30.3420	30.34430	33.2873	33.28938	43.5259	43.52787
$p_z = 0.5$	42.7204	42.7241	44.3903	44.39376	46.1197	46.12296	49.7272	49.73018	61.0459	61.04855
$p_z = 1$	55.5528	55.55739	57.3187	57.32303	59.1129	59.11699	62.7549	62.75864	73.5496	73.55288
$p_z = 2$	71.1944	71.20037	72.7684	72.77410	74.3479	74.35345	77.5097	77.51483	86.6972	86.70173
$p_z = 5$	84.2237	84.2319	85.5610	85.56895	86.9181	86.92588	89.6680	89.67549	97.7267	97.73379

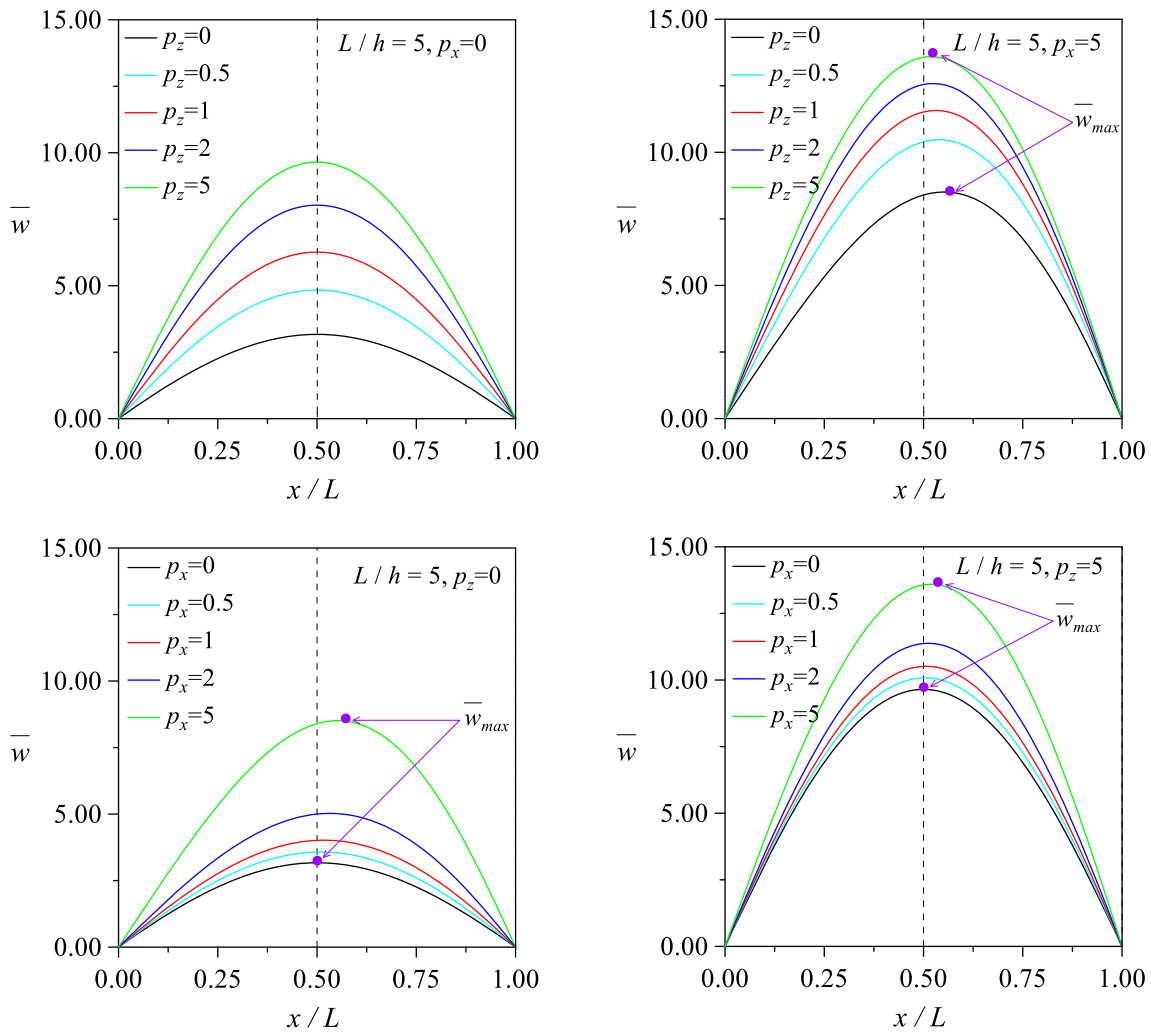


Fig. 3 Normalized transverse deflections of the SS 2D-FGBs with respect to the normalized coordinate x/L for various gradation exponents ($u^0 \neq 0$)

very close to the mid-section. For $p_x = 0$, the location of the normalized maximum transverse deflections is at the mid-section ($x/L = 0.5$). As seen, with the increase of p_x , x/L also increases. Also, when p_z increases for $p_x = 5$, x/L decreases.

Figure 4 shows normalized axial stress of the SS 2D-FGBs with respect to the normalized thickness z/h and the normalized coordinate x/L for various gradation exponents. When p_x and p_z increase, the ceramic ratio of the beam decreases, and the metal ratio increases. Based on this information, the following comments can be made. In any beam cross section in the x -direction, the tensile region is at the top, and the compression region is at the bottom. As it is expected, the normalized absolute maximum stress is at the top surface of the beam. It is clear that the tensile stress increase by increasing of gradation exponent in the z -direction. As it increases p_x , the maximum axial stress decrease, and it moves away from the middle section.

In Fig. 5, normalized shear stress of the SS 2D-FGBs with respect to the normalized thickness z/h and the normalized coordinate x/L for various gradation exponents are presented. The shear stress distribution is linear for $p_z = 0$. For nonzero values of p_z , for example, with increasing p_x for $p_z = 1$, shear stress does not change at the left edge of the beam, while shear stress decreases at the right edge. The reason for this is that with the increase in p_x , the material property of the left edge does not change, while the material property of the right edge approaches metal. When p_x is constant, shear stress increases at the top of the section with increasing p_z . It is observed that the variation of p_z is more effective on shear stress than the p_x .

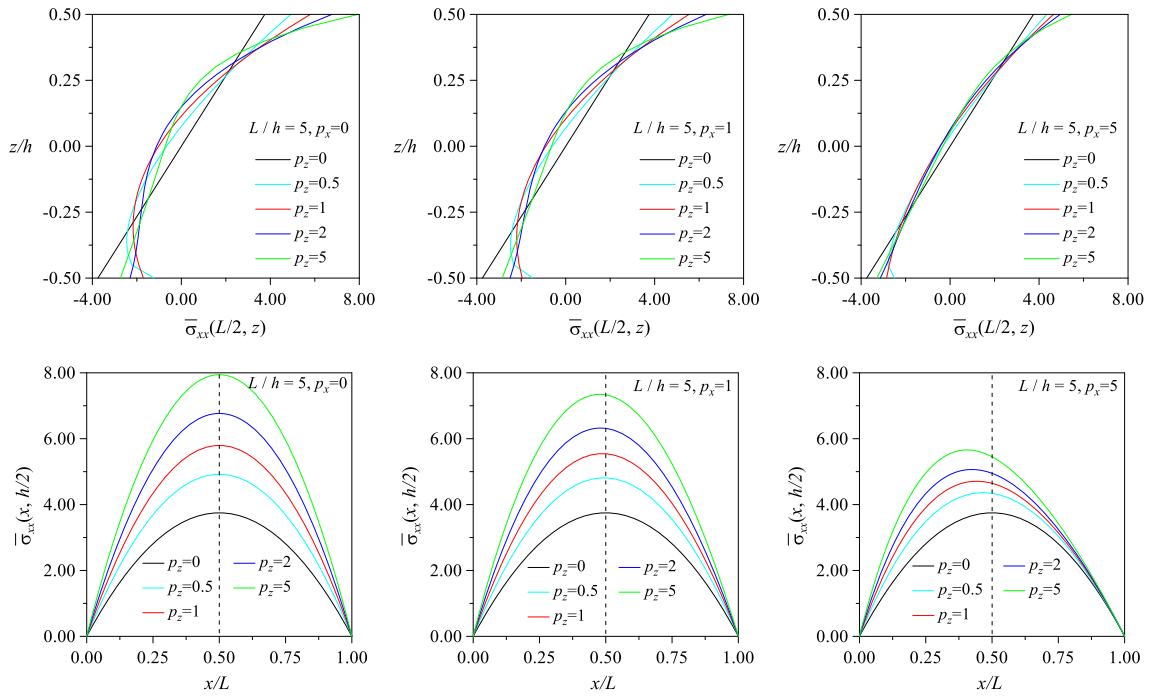


Fig. 4 Normalized axial stress of the SS 2D-FGBs with respect to the normalized thickness z/h and the normalized coordinate x/L for various gradation exponents ($u^0 \neq 0, L/h = 5$)

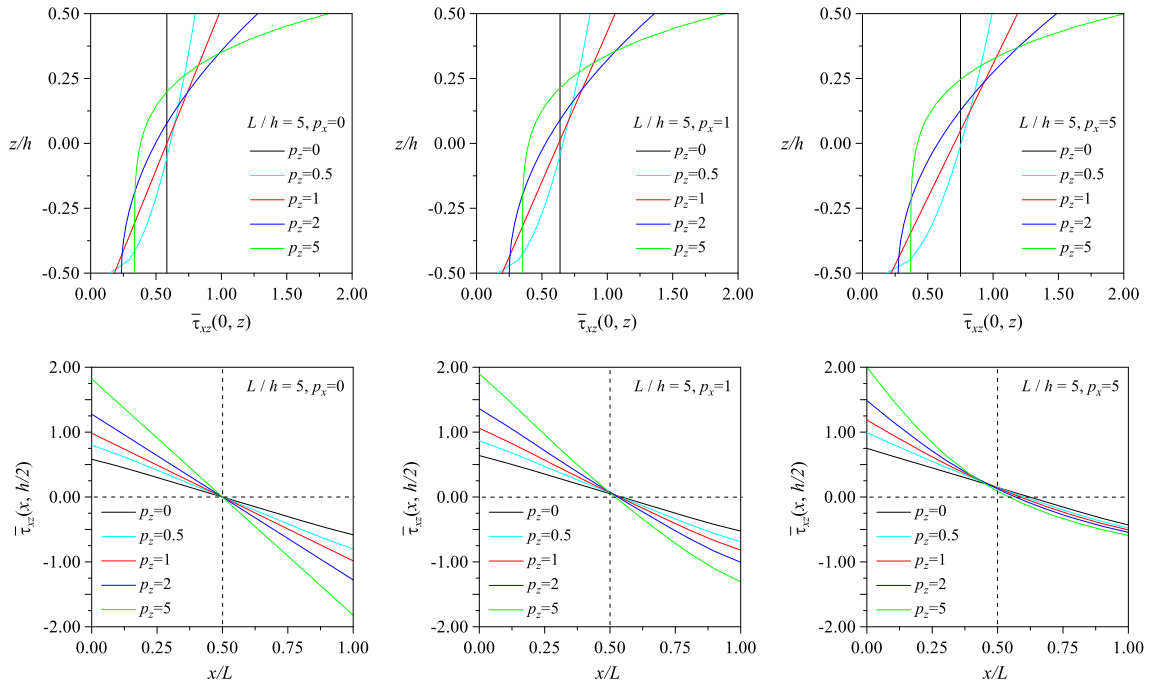


Fig. 5 Normalized shear stress of the SS 2D-FGBs with respect to the normalized thickness z/h and the normalized coordinate x/L for various gradation exponents ($u^0 \neq 0, L/h = 5$)

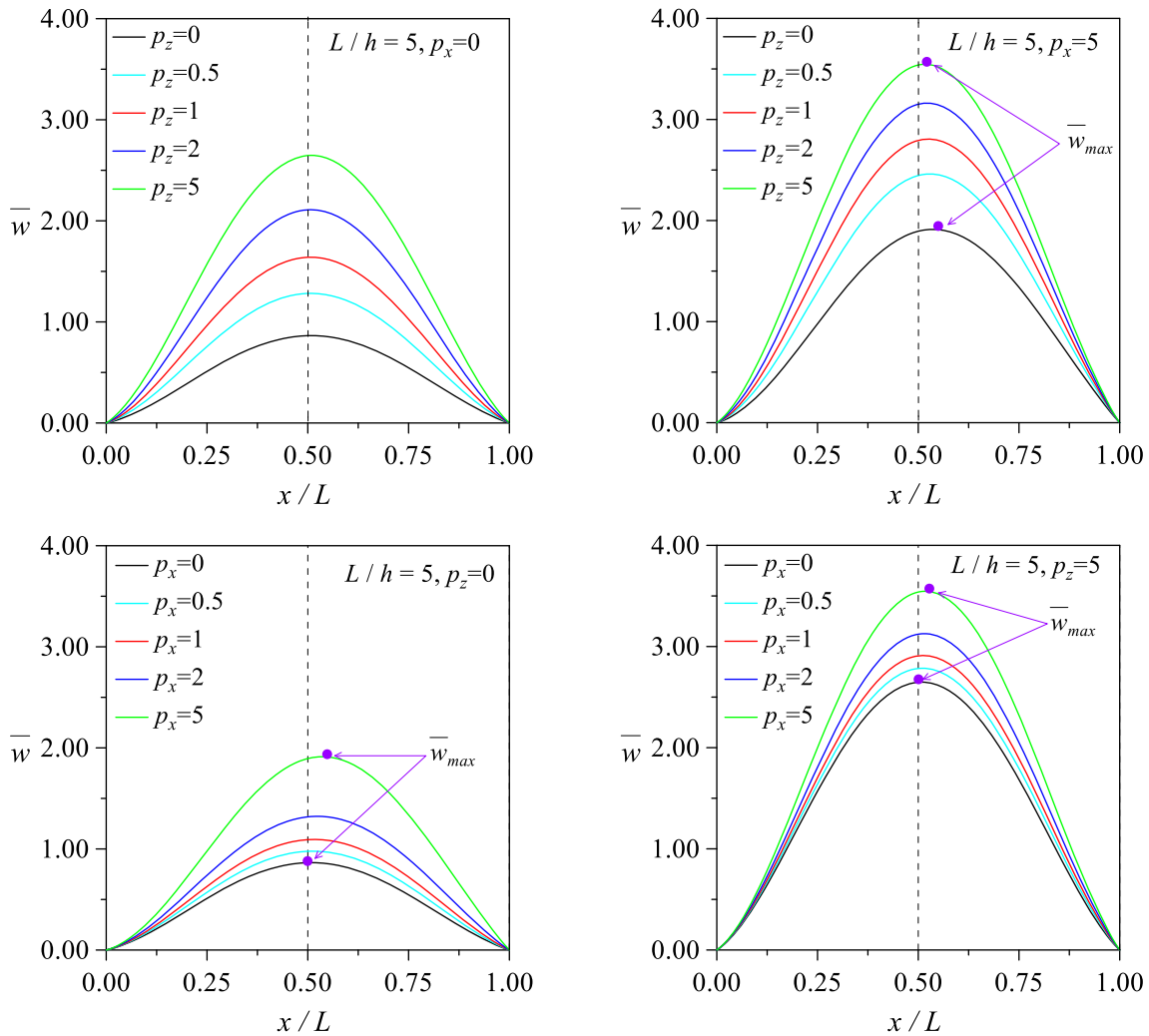


Fig. 6 Normalized transverse deflections of the CC 2D-FGBs with respect to the normalized coordinate x/L for various gradation exponents ($u^0 \neq 0$)

Figure 6 shows normalized transverse deflections of the CC 2D-FGBs with respect to the normalized coordinate x/L for various gradation exponents. The normalized transverse deflections increase with increasing p_x and p_z (i.e., decreasing the ceramic ratio of the beam). For $p_x = 0$, while the maximum deflection is in the middle section of the beam, it moves away from the middle section with the increase of p_x . The comments for the SS beam can be said for this as well.

In Fig. 7, the normalized axial stress of the CC 2D-FGBs with respect to the normalized thickness z/h and the normalized coordinate x/L for various gradation exponents is presented. At different values of p_x and p_z , the compression region is above the section at the left and right edges of the beam. In the middle region of the beam (approximately $0.25 \leq x/L \leq 0.8$), the tensile region is above the section. The maximum compressive stress occurs at the $x/L = 0$ and $z/h = 0.5$ point of the beam. Here, the material property is ceramic. The maximum compressive stress increases with the increase of p_x and p_z . The tensile stress decreases with increasing p_x in the middle section of the beam $x/L = 0.5$. Here, with the rise of p_z , the tensile stress increases.

The variations of the normalized shear stress of the CC 2D-FGBs with respect to the normalized thickness z/h and the normalized coordinate x/L for various gradation exponents are given in Fig. 8. For $p_x = 0$ and $p_z = 0$, the shear stress is zero in the middle section. The shear stress increases at the left edge and decreases at the right edge with the increase in p_x . Here, the material property is ceramic on the left edge, and the ceramic ratio decreases toward the right end of the beam with the increase in p_x . When p_x is not changed, the maximum shear stress increases with the increase of p_z on the left and right edges.

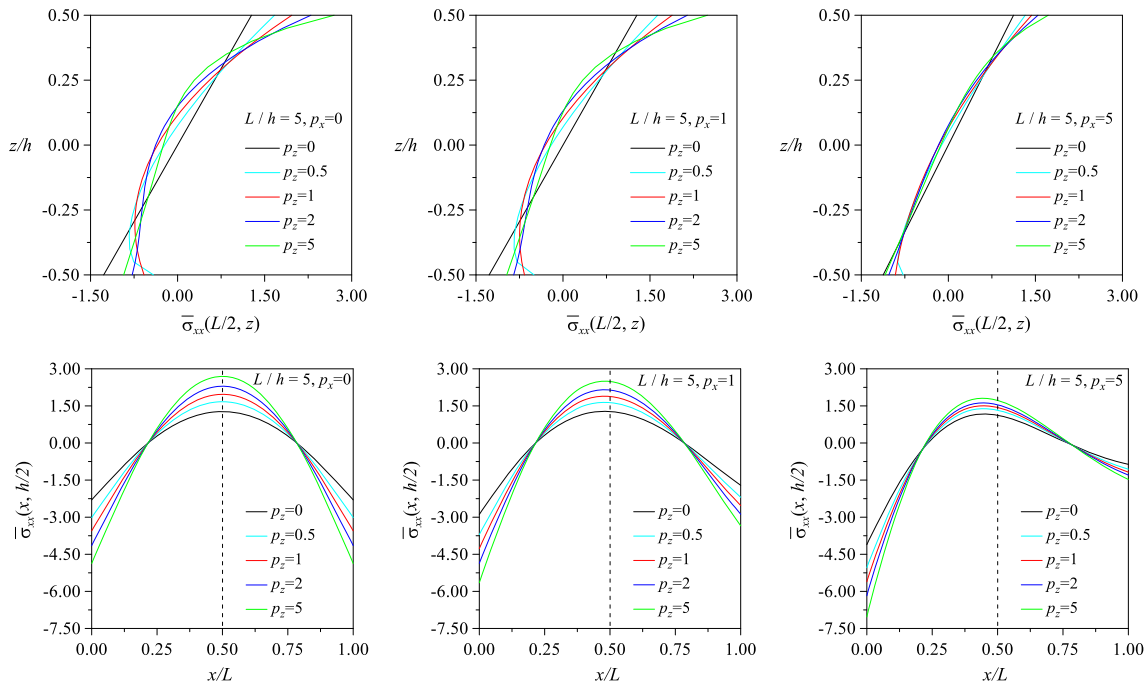


Fig. 7 Normalized axial stress of the CC 2D-FGBs with respect to the normalized thickness z/h and the normalized coordinate x/L for various gradation exponents ($u^0 \neq 0, L/h = 5$)

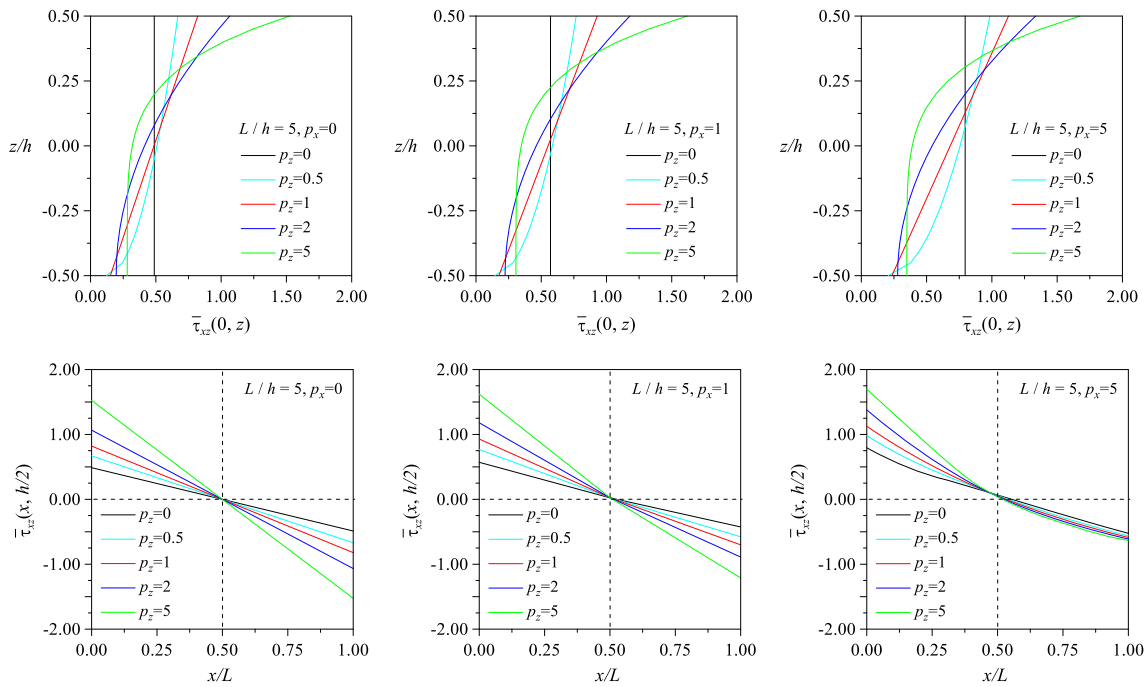


Fig. 8 Normalized shear stress of the CC 2D-FGBs with respect to the normalized thickness z/h and the normalized coordinate x/L for various gradation exponents ($u^0 \neq 0, L/h = 5$)

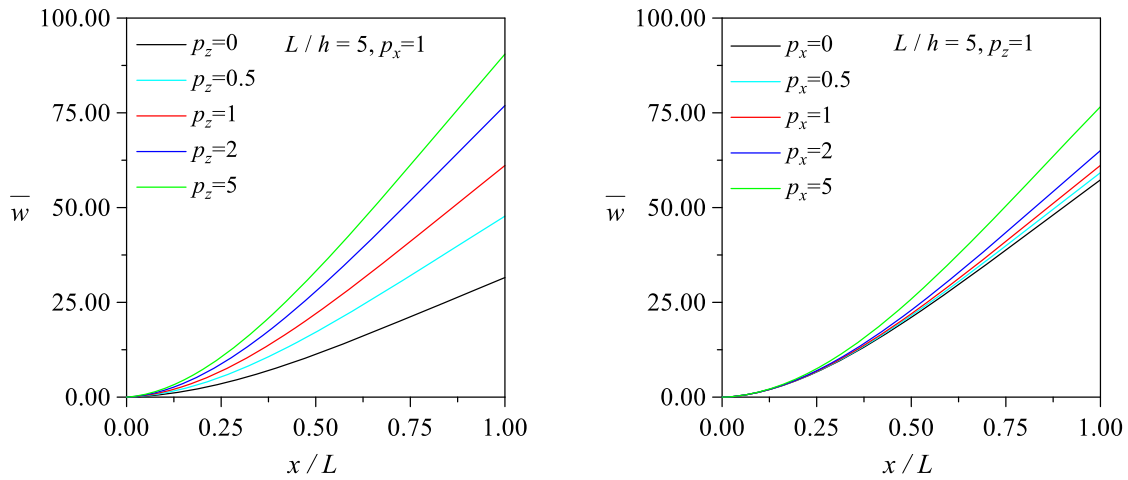


Fig. 9 Normalized transverse deflections of the CF 2D-FGBs with respect to the normalized coordinate x/L for various gradation exponents ($u^0 \neq 0$)

In Fig. 9, the normalized transverse deflections of the CF 2D-FGBs are plotted for various p_x and p_z . The gradation exponents in x , z -direction p_x , and p_z are set to 1. The effect of the varying gradation exponents in the x , z -direction p_x , and p_z is observed for the transverse deflections. As the gradation exponent in the x and z -direction increases, the deflections increase. As expected, the increase in p_z affects the deflections more than p_x . The maximum deflections occur at the largest value of p_z (high metal content of the beam). The maximum deflections always occur at the free end of the beam, regardless of material properties.

The variations of the normalized axial stress of the CF 2D-FGBs with respect to the normalized thickness z/h and the normalized coordinate x/L for various gradation exponents are given in Fig. 10. When p_x increases, the material property on the left edge does not change, so there is not much change in axial stress. For example, for $p_z = 0, 1, 2$, and 5 , the variation of p_x does not affect their magnitudes, as the maximum compressive stress occurs at the left edge. However, the variation of p_x changes the axial stress distribution in the x , and z -direction of the beam. The compressive stresses increase with the increase of p_z . In addition, in any beam cross section in the x -direction, the compression region is at the top, and the tensile region is at the bottom. As is expected, the normalized absolute maximum stress is generally at the top surface of the beam.

The variations of the normalized shear stress of the CF 2D-FGBs with respect to the normalized thickness z/h and the normalized coordinate x/L for various gradation exponents are shown in Fig. 11. Since the maximum shear stress is on the left edge, increasing p_x does not change the value of the maximum shear stress. The maximum shear stress increases with the increase of p_z . Here, it is seen that p_z is more effective on shear stress.

4 Conclusion

A Navier’s method based on FSDT is presented for bending analysis of the 2D-FGBs subjected to various sets of boundary conditions. In Navier’s method, different trigonometric series functions are proposed for each boundary condition. The governing equations are derived according to Lagrange’s principle. The variation of the components of the beam material in the volume is defined by a power-law rule. The normalized maximum transverse deflections, the normalized axial and transverse shear stresses are obtained for various boundary conditions, gradation exponents (p_x, p_z) in the x - and z -directions, and the slenderness (L/h). The results show that the gradation exponents, as well as the boundary conditions, play a significant influence on the bending behavior of the 2D-FGBs. According to the study, the following conclusions can be drawn:

- The trigonometric series functions used in the study can accurately predict the transverse deflections and the stresses of 2D-FGBs with different boundary conditions. The accuracy and performance of the present solution in the computation are well enough.
- The transverse deflections increase when the p_x and p_z increase in both directions (i.e., ceramic ratio decreases).
- The location of the maximum deflection in the SS and CC beams depends on the material property (depend on p_x and p_z).

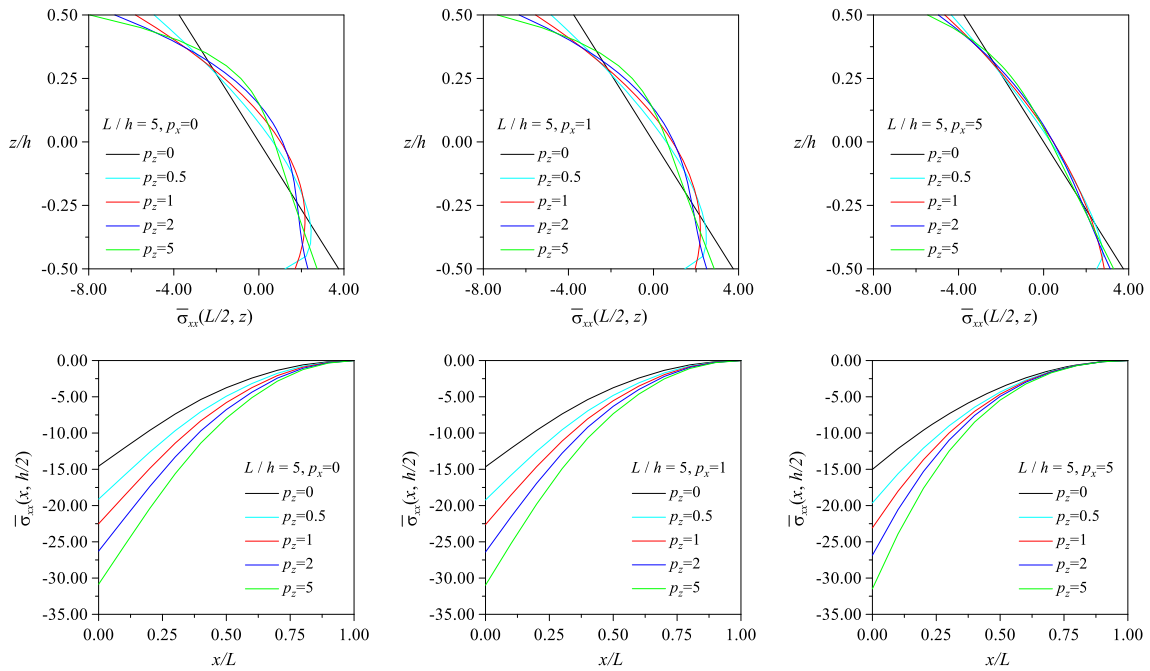


Fig. 10 Normalized axial stress of the CF 2D-FGBs with respect to the normalized thickness z/h and the normalized coordinate x/L for various gradation exponents ($u^0 \neq 0, L/h = 5$)

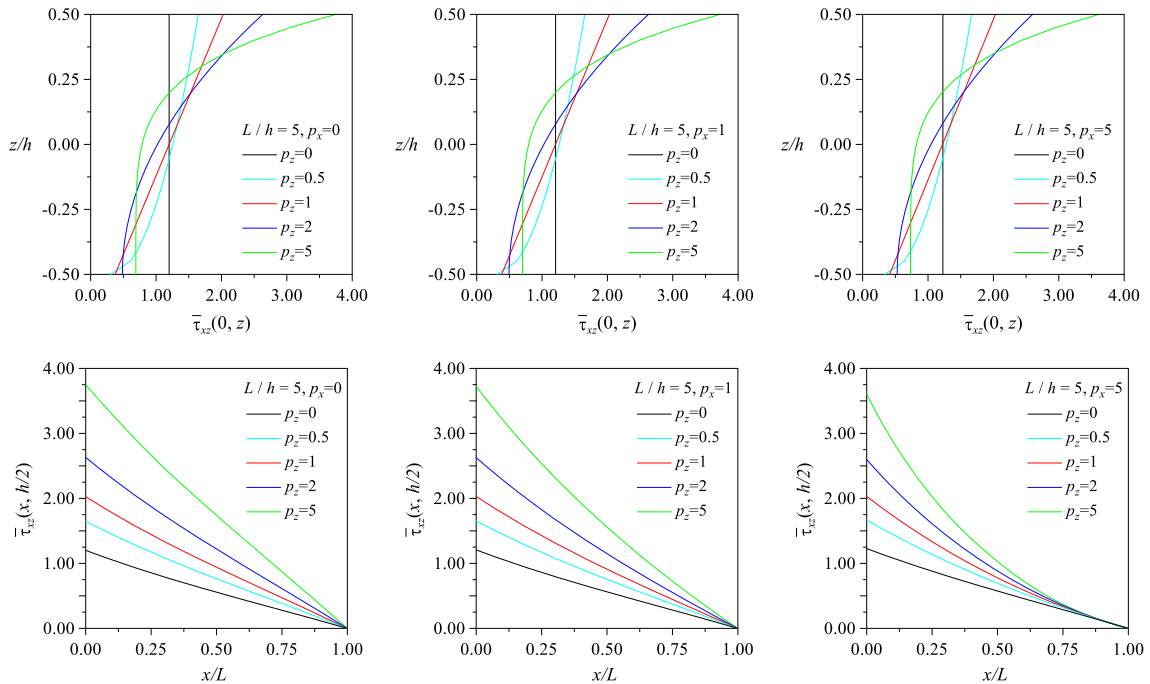


Fig. 11 Normalized shear stress of the CF 2D-FGBs with respect to the normalized thickness z/h and the normalized coordinate x/L for various gradation exponents ($u^0 \neq 0, L/h = 5$)

- In CF beams, it has been observed that the material property has no effect on the location of the maximum deflection, but it is quite effective on the magnitude of the maximum deflection.
- Since p_z changes the material properties faster, the variation of p_z is more effective on stresses than the p_x .

Declarations

Conflict of interest The authors declare that they have no known competing financial interests or personal relationships that could have appeared to influence the work reported in this paper.

References

1. Chakraborty, A., Gopalakrishnan, S., Reddy, J.N.: A new beam finite element for the analysis of functionally graded materials. *Int J Mech Sci.* **45**, 519–39 (2003)
2. Aydogdu, M., Taskin, V.: Free vibration analysis of functionally graded beams with simply supported edges. *Mater Des.* **28**, 1651–1656 (2007)
3. Li, X.F.: A unified approach for analyzing static and dynamic behaviors of functionally graded Timoshenko and Euler-Bernoulli beams. *J Sound Vib.* **318**, 1210–1229 (2008)
4. Li, X.F., Wang, B.L., Han, J.C.: A higher-order theory for static and dynamic analyses of functionally graded beams. *Arch Appl Mech.* **80**, 1197–1212 (2010)
5. Nguyen, T.K., Vo, T.P., Thai, H.T.: Static and free vibration of axially loaded functionally graded beams based on the first-order shear deformation theory. *Compos Part B Eng.* **55**, 147–157 (2013)
6. Vo, T.P., Thai, H.T., Nguyen, T.K., Inam, F., Lee, J.: Static behaviour of functionally graded sandwich beams using a quasi-3D theory. *Compos Part B Eng.* **68**, 59–74 (2015)
7. Huang, Y., Zhang, M., Rong, H.: Buckling analysis of axially functionally graded and non-uniform beams based on Timoshenko theory. *Acta Mech Solida Sin.* **29**, 200–207 (2016)
8. Kahya, V., Turan, M.: Finite element model for vibration and buckling of functionally graded beams based on the first-order shear deformation theory. *Compos Part B Eng.* **109**, 108–115 (2017)
9. Kahya, V., Turan, M.: Vibration and stability analysis of functionally graded sandwich beams by a multi-layer finite element. *Compos Part B Eng.* **146**, 198–212 (2018)
10. Turan, M., Kahya, V.: Free vibration and buckling analysis of functionally graded sandwich beams by Navier's method. *J Fac Eng Archit Gazi Univ.* **36**, 743–757 (2021)
11. Bouafia, K., Selim, M.M., Bourada, F., Bousahla, A.A., Bourada, M., Tounsi, A., Adda Bedia, E.A., Tounsi, A.: Bending and free vibration characteristics of various compositions of FG plates on elastic foundation via quasi 3D HSDT model. *Steel Compos. Struct.* **41**, 487–503 (2021)
12. Tahir, S.I., Chikh, A., Tounsi, A., Al-Osta, M.A., Al-Dulaijan, S.U., Al-Zahrani, M.M.: Wave propagation analysis of a ceramic-metal functionally graded sandwich plate with different porosity distributions in a hygro-thermal environment. *Compos. Struct.* **269**, 114030 (2021)
13. Mudhaffar, I.M., Tounsi, A., Chikh, A., Al-Osta, M.A., Al-Zahrani, M.M., Al-Dulaijan, S.U.: Hygro-thermo-mechanical bending behavior of advanced functionally graded ceramic metal plate resting on a viscoelastic foundation. *Structures.* **33**, 2177–2189 (2021)
14. Kouider, D., Kaci, A., Selim, M.M., Bousahla, A.A., Bourada, F., Tounsi, A., Tounsi, A., Hussain, M.: An original four-variable quasi-3D shear deformation theory for the static and free vibration analysis of new type of sandwich plates with both FG face sheets and FGM hard core. *Steel Compos. Struct.* **41**, 167–191 (2021)
15. Hachemi, H., Bousahla, A.A., Kaci, A., Bourada, F., Tounsi, A., Benrahou, K.H., Tounsi, A., Al-Zahrani, M.M., Mahmoud, S.R.: Bending analysis of functionally graded plates using a new refined quasi-3D shear deformation theory and the concept of the neutral surface position. *Steel Compos. Struct.* **39**, 51–64 (2021)
16. Bakoura, A., Bourada, F., Bousahla, A.A., Tounsi, A., Benrahou, K.H., Tounsi, A., Al-Zahrani, M.M., Mahmoud, S.R.: Buckling analysis of functionally graded plates using HSDT in conjunction with the stress function method. *Comput. Concr.* **27**, 73–83 (2021)
17. Rachid, A., Ouinas, D., Lousdad, A., Zaoui, F.Z., Achour, B., Gsmi, H., Butt, T.A., Tounsi, A.: Mechanical behavior and free vibration analysis of FG doubly curved shells on elastic foundation via a new modified displacements field model of 2D and quasi-3D HSDTs. *Thin-Walled Struct.* **172**, 108783 (2022)
18. Zaitoun, M.W., Chikh, A., Tounsi, A., Al-Osta, M.A., Sharif, A., Al-Dulaijan, S.U., Al-Zahrani, M.M.: Influence of the visco-Pasternak foundation parameters on the buckling behavior of a sandwich functional graded ceramic-metal plate in a hygrothermal environment. *Thin-Walled Struct.* **170**, 108549 (2022)
19. Karamanli, A., Vo, T.P.: Size dependent bending analysis of two directional functionally graded microbeams via a quasi-3D theory and finite element method. *Compos Part B Eng.* **144**, 171–183 (2018)
20. Chinh, N.V., Inh, L.C., Ngoc Anh, L.T.: Elastostatic bending of a 2D-FGSW beam under nonuniform distributed loads. *Vietnam J Sci Technol.* **57**, 381–400 (2019)
21. Chen, D., Zheng, S., Wang, Y., Yang, L., Li, Z.: Nonlinear free vibration analysis of a rotating two-dimensional functionally graded porous micro-beam using isogeometric analysis. *Eur J Mech A/Solids.* **84**, 104083 (2020)
22. Nguyen, D.K., Vu, A.N.T., Le, N.A.T., Pham, V.N.: Dynamic behavior of a bidirectional functionally graded sandwich beam under nonuniform motion of a moving load. *Shock Vib.* (2020). <https://doi.org/10.1155/2020/8854076>

23. Viet, N.V., Zaki, W., Wang, Q.: Free vibration characteristics of sectioned unidirectional/bidirectional functionally graded material cantilever beams based on finite element analysis. *Appl Math Mech (English Ed)*. **41**, 1787–1804 (2020)
24. Le, C.I., Le, N.A.T., Nguyen, D.K.: Free vibration and buckling of bidirectional functionally graded sandwich beams using an enriched third-order shear deformation beam element. *Compos Struct*. **261**, 113309 (2021)
25. Lü, C.F., Chen, W.Q., Xu, R.Q., Lim, C.W.: Semi-analytical elasticity solutions for bi-directional functionally graded beams. *Int J Solids Struct*. **45**, 258–275 (2008)
26. Şimşek, M.: Bi-directional functionally graded materials (BDFGMs) for free and forced vibration of Timoshenko beams with various boundary conditions. *Compos Struct*. **133**, 968–978 (2015)
27. Şimşek, M.: Buckling of Timoshenko beams composed of two-dimensional functionally graded material (2D-FGM) having different boundary conditions. *Compos Struct*. **149**, 304–314 (2016)
28. Nejad, M.Z., Hadi, A., Rastgoo, A.: Buckling analysis of arbitrary two-directional functionally graded Euler-Bernoulli nano-beams based on nonlocal elasticity theory. *Int J Eng Sci*. **103**, 1–10 (2016)
29. Wang, Z.H., Wang, X.H., Xu, G.D., Cheng, S., Zeng, T.: Free vibration of two-directional functionally graded beams. *Compos Struct*. **135**, 191–198 (2016)
30. Karamanli, A.: Bending behaviour of two directional functionally graded sandwich beams by using a quasi-3d shear deformation theory. *Compos Struct*. **174**, 70–86 (2017)
31. Karamanli, A.: Elastostatic analysis of two-directional functionally graded beams using various beam theories and Symmetric Smoothed Particle Hydrodynamics method. *Compos Struct*. **160**, 653–669 (2017)
32. Karamanli, A.: Bending analysis of two directional functionally graded beams using a four-unknown shear and normal deformation theory. *J Polytech*. **21**, 861–874 (2018)
33. Karamanli, A.: Free vibration and buckling analysis of two directional functionally graded beams using a four-unknown shear and normal deformable beam theory. *Anadolu Univ J Sci Technol A - Appl Sci Eng*. **19**, 375–406 (2018)
34. Karamanli, A.: Free vibration analysis of two directional functionally graded beams using a third order shear deformation theory. *Compos Struct*. **189**, 127–136 (2018)
35. Karamanli, A.: Analytical solutions for buckling behavior of two directional functionally graded beams using a third order shear deformable beam theory. *Acad Platf J Eng Sci*. **6**, 164–178 (2018)
36. Shanab, R.A., Attia, M.A.: Semi-analytical solutions for static and dynamic responses of bi-directional functionally graded nonuniform nanobeams with surface energy effect. *Engineering with Computers* (2020). <https://doi.org/10.1007/s00366-020-01205-6>
37. Huang, Y.: Bending and free vibrational analysis of bi-directional functionally graded beams with circular cross-section. *Appl Math Mech*. **41**, 1497–1516 (2020)
38. Huang, Y., Ouyang, Z.Y.: Exact solution for bending analysis of two-directional functionally graded Timoshenko beams. *Arch Appl Mech*. **90**, 1005–1023 (2020)
39. Nguyen, T.K., Nguyen, N.D., Vo, T.P., Thai, H.T.: Trigonometric-series solution for analysis of laminated composite beams. *Compos Struct*. **160**, 142–151 (2017)
40. MATLAB (matrix laboratory), MathWorks, USA (2016)